JGR Oceans

RESEARCH ARTICLE
10.1029/2019JC015109

Special Section:
Forum for Arctic Modeling and Observational Synthesis (FAMOS) 2: Beaufort Gyre phenomenon

Inorganic Carbon and pCO_2 Variability During Ice Formation in the Beaufort Gyre of the Canada Basin

Michael D. DeGrandpre[1], Chun-Ze Lai[1], Mary-Louise Timmermans[2], Richard A. Krishfield[3], Andrey Proshutinsky[3], and Daniel Torres[3]

[1]Department of Chemistry and Biochemistry, University of Montana, Missoula, MT, USA, [2]Department of Geology and Geophysics, Yale University, New Haven, CT, USA, [3]Woods Hole Oceanographic Institution, Woods Hole, MA, USA

Key Points:
- We deployed a pCO_2 sensor in the northwest Canada Basin of the Arctic Ocean; the time series shows a steady increase from fall to winter
- The pCO_2 increase is attributed to sea ice formation that excludes inorganic carbon; the inorganic carbon concentrated in the mixed layer
- Ice exclusion of inorganic carbon could become an increasingly important part of the Arctic Ocean carbon cycle with diminishing ice cover

Correspondence to:
M. D. DeGrandpre,
michael.degrandpre@umontana.edu

Citation:
DeGrandpre, M. D., Lai, C.-Z., Timmermans, M.-L., Krishfield, R. A., Proshutinsky, A., & Torres, D. (2019). Inorganic Carbon and pCO_2 Variability During Ice Formation in the Beaufort Gyre of the Canada Basin. *Journal of Geophysical Research: Oceans*, *124*, 4017–4028. https://doi.org/10.1029/2019JC015109

Received 28 FEB 2019
Accepted 1 MAY 2019
Accepted article online 7 MAY 2019
Published online 21 JUN 2019

Abstract Solute exclusion during sea ice formation is a potentially important contributor to the Arctic Ocean inorganic carbon cycle that could increase as ice cover diminishes. When ice forms, solutes are excluded from the ice matrix, creating a brine that includes dissolved inorganic carbon (DIC) and total alkalinity (A_T). The brine sinks, potentially exporting DIC and A_T to deeper water. This phenomenon has rarely been observed, however. In this manuscript, we examine a ~1 year pCO_2 mooring time series where a ~35-μatm increase in pCO_2 was observed in the mixed layer during the ice formation period, corresponding to a simultaneous increase in salinity from 27.2 to 28.5. Using salinity and ice based mass balances, we show that most of the observed increases can be attributed to solute exclusion during ice formation. The resulting pCO_2 is sensitive to the ratio of A_T and DIC retained in the ice and the mixed layer depth, which controls dilution of the ice-derived A_T and DIC. In the Canada Basin, of the ~92 μmol/kg increase in DIC, 17 μmol/kg was taken up by biological production and the remainder was trapped between the halocline and the summer stratified surface layer. Although not observed before the mooring was recovered, this inorganic carbon was likely later entrained with surface water, increasing the pCO_2 at the surface. It is probable that inorganic carbon exclusion during ice formation will have an increasingly important influence on DIC and pCO_2 in the surface of the Arctic Ocean as seasonal ice production and wind-driven mixing increase with diminishing ice cover.

Plain Language Summary When sea ice forms, the dissolved solutes are squeezed out of the ice matrix, forming a dense brine that can sink into deeper water. This process has a potentially important role in the inorganic carbon cycle because dissolved inorganic carbon can sink with the brine, exporting it from the surface ocean and increasing the sea surface CO_2 partial pressure (pCO_2). We deployed a pCO_2 sensor at 30-m depth in the Canada Basin, the largest of the Arctic Ocean subbasins, that documented an increase in pCO_2 during the fall to winter ice formation period. This increase correlated with an increase in salinity over the same time period. A simple model calculation supports that the increase in pCO_2 and inorganic carbon is primarily due to ice formation. This finding has important implications for the future inorganic carbon cycle as seasonal ice formation increases due to loss of perennial ice cover in the Arctic.

1. Introduction

The Arctic Ocean (AO) carbon cycle is changing. With diminishing ice cover, the air-sea exchange of heat, momentum, and mass have increased in the AO, all of which are important regulators of the ocean carbon cycle. Loss of sea ice has increased air-sea CO_2 fluxes (Bates et al., 2006; Jutterström & Anderson, 2010; Yasunaka et al., 2016) by exposure to high CO_2 levels in the atmosphere and increased turbulent exchange from winds and waves. While the AO is an overall sink of atmospheric CO_2, warming is reducing the uptake by increasing pCO_2 in the sea surface (Cai et al., 2010; DeGrandpre et al., 2019; Else et al., 2013). Exposure of the AO surface water to high anthropogenic atmospheric CO_2 levels has accelerated ocean acidification (Robbins et al., 2013; Yamamoto-Kawai et al., 2011). Biological production is also changing with complex tradeoffs between increased light penetration and reduced nutrient fluxes. Satellite data reveal a steady increase in primary production (Arrigo & van Dijken, 2015), while other studies have shown a decrease due to freshwater stratification (Bergeron & Tremblay, 2014). How these changes in biological production are affecting carbon uptake and export, that is, the biological pump, remain unknown (Anderson & Macdonald, 2015).

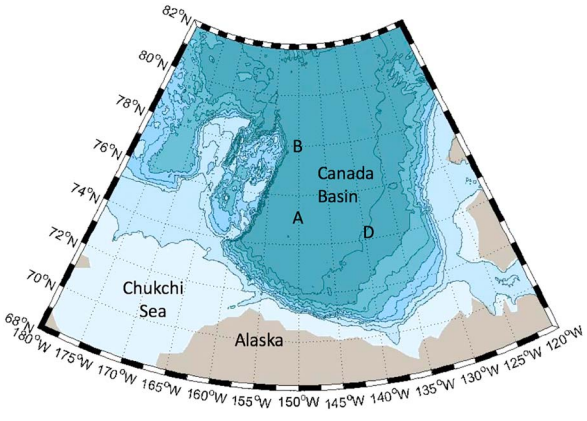

Figure 1. Beaufort Gyre Observing System mooring locations in the Canada Basin (A, B, D). This study is focused on a pCO_2 record collected at ~30-m depth on Mooring B (78.01°N, 150.00°W, 3,830-m total water depth). The mooring was deployed on 9 October 2014 and recovered on 29 September 2015 (collecting data for 356 days).

Ice formation is another process that could potentially alter the AO carbon cycle. Specifically, salt and other solutes are excluded from the crystal lattice when seawater freezes, a process called "ice exclusion" or "solute exclusion" (Petrich & Eicken, 2010). The cold, dense brine that forms from this process is an important mechanism for deep mixing in widespread areas of the oceans (Shcherbina et al., 2003). Ice exclusion can increase dissolved O_2 (Timmermans et al., 2010) and dissolved inorganic carbon (DIC) in the surface mixed layer (Rysgaard et al., 2007, 2011). The freezing process can also lead to the formation of ikaite, an abiotic form of calcium carbonate (Dieckmann et al., 2008; Rysgaard et al., 2012). Exclusion of inorganic carbon has been verified in both laboratory (Geilfus et al., 2016) and field studies of sea ice formation (Fransson et al., 2013; Rysgaard et al., 2007). In a study in the Amundsen Gulf, a seasonal increase in both sea surface pCO_2 and salinity was attributed to brine exclusion during ice formation (Else et al., 2012). Entrainment of DIC and total alkalinity (A_T) in dense brines might have contributed significantly to inorganic carbon export and atmospheric CO_2 drawdown during the last glacial period (Bouttes et al., 2010). Models of contemporary ice formation estimate a small net export of DIC and A_T to depth for all polar regions but with a high degree of uncertainty (Moreau et al., 2016). Stratification is the main factor that limits export. Rysgaard et al. (2011) assumed the DIC would be entrained below the mixed layer, whereas Moreau et al. (2016) found that the DIC does not penetrate sufficiently deep to be sequestered. Dissolution of ikaite during ice melt is thought to lower sea surface pCO_2 in the AO (Rysgaard et al., 2013). It could, however, also sink below the mixed layer and export DIC and A_T more efficiently but this has never been verified (Geilfus et al., 2016). As larger areas of the AO become ice free in summer, these sea ice related inorganic carbon fluxes and exports are no longer limited to coastal areas, but also become enhanced over the deep basins of the AO. Thus, it is important to better understand this potentially important process. There have been few direct observations of the inorganic carbon flux from brine exclusion, however, because inorganic measurements are rarely made in the fall and winter when sea ice growth is maximal.

To address this sampling gap, we have been deploying pCO_2 and pH sensors on year-round moorings and ice-tethered profilers (ITPs; Krishfield et al., 2008; Toole et al., 2011) in the Canada Basin since 2012 (Islam et al., 2016, 2017). This study focuses on a pCO_2 time series recorded on a subsurface mooring at ~30-m depth from October 2014 to September 2015 in the northwest Canada Basin (Figure 1). We use mass balance models based on both changes in salinity and ice thickness to predict changes in DIC and A_T. The modeled pCO_2 and DIC support that the observed increase in mixed layer pCO_2 is due to ice formation.

2. Methods

2.1. Mooring and Instrument Descriptions

The Canada Basin has been the focus of repeated hydrographic cruises since 2003 as part of the U.S. Beaufort Gyre Exploration Project on the Canadian icebreaker CCGS Louis S. St. Laurent (Proshutinsky et al., 2009; http://www.whoi.edu/beaufortgyre/). Originally four and now three moorings along with ITPs have been deployed annually during these cruises (Figure 1; Krishfield et al., 2008, 2014). The standard mooring configuration consists of a subsurface float with integrated 420-kHz upward looking sonar (ULS; IPS4, ASL Environmental Sciences) and 600-kHz upward looking acoustic Doppler current profiler (ADCP; Workhorse, RD Instruments), a profiler (McLane Moored Profiler, MMP), dual acoustic releases, and a bottom pressure recorder (SBE-16plus BPR, Seabird Electronics, Inc.) immediately above the anchor. The MMP records currents and hydrographic data from 40 to 50 m down to 1,500- to 2,050-m depth depending on the mooring configuration. Mooring B was also equipped with a conductivity-temperature-depth (CTD) sensor (SeaBird MicroCAT) located 1 m below the subsurface float and a partial pressure of CO_2 (pCO_2) sensor

(Submersible Autonomous Moored Instruments-CO_2, Sunburst Sensors; DeGrandpre et al., 1995) directly below the CTD at 30 m.

The Submersible Autonomous Moored Instruments sensor recorded pCO_2 and temperature at 2-hr intervals. Before deployment, the sensor was calibrated at ~1 °C over the expected pCO_2 range (200–450 μatm). The calibration was corrected to the in situ temperature as described in DeGrandpre et al. (1995). The pCO_2 data were quality controlled using shipboard underway pCO_2 or samples collected before and after deployment (see below). Ice draft was quantified to within ±10 cm using the ULS data and converted to ice thickness using the scaling factor of 1.123 (Krishfield et al., 2014). Unfortunately, the MMP did not function during the 2014 deployment.

2.2. Other Supporting Data

The CO_2 species can be quantified using two inorganic carbon parameters. In this study only pCO_2 was measured but others have shown that A_T is closely correlated with salinity in the Canada Basin (Yamamoto-Kawai et al., 2005). A linear correlation between A_T and salinity (S) was obtained using CCGS Louis S. St. Laurent shipboard measurements from 41 stations in the Canada Basin between 2013 and 2017 (depth range 0–50 m, salinity range ~25.5–30.5). The total alkalinity (A_{Tsalin}) was then estimated using this correlation ($r^2 = 0.88$, $n = 284$, residual standard deviation ±38 μmol/kg):

$$A_{Tsalin} = 60.268 \times S + 333.64 \quad (1)$$

Importantly, based on this correlation salinity captures the major variability in A_T found in the seasonal pycnocline and mixed layer (0–50 m) and any trend in fall/winter salinity would therefore be expected to be mirrored by A_T. The ±38 μmol/kg scatter in the linear fit, some of which might originate from erroneous A_T data, does not result in similar uncertainty in A_{Tsalin}. DIC and other inorganic carbon parameters were calculated using pCO_2, A_{Tsalin}, temperature, and salinity in the equilibrium program CO2SYS (Pierrot et al., 2006) with the Mehrbach et al. (1973) constants refit by Dickson and Millero (1987). Evans et al. (2015) found that these constants estimate pCO_2 in AO surface waters to within ±10 μatm of the measured value when using A_T and DIC, comparable to other equilibrium constants. Nutrients that contribute to total alkalinity were assumed to be negligible in the CO2SYS calculations.

2.3. Modeling

Different mass balances based on salinity and sea ice thickness were used to estimate contributions of ice formation to mixed layer pCO_2 variability. In the salinity balance, we assume that when brine sinks it mixes with the surrounding water until density between the brine and surrounding seawater are equal. Under growing sea ice away from polynya regions, brine is rejected in insufficient volumes to penetrate the base of the mixed layer after entraining the less dense ambient water (Moreau et al., 2016). The general picture is one of an increasingly salty mixed layer over the course of winter and fall, where a portion of the excess salt results from sea ice growth. Thus, salinity can be used as a conservative tracer to quantify the amount of A_T and DIC that concentrates in the mixed layer during ice formation, neglecting lateral advection and vertical entrainment of salinity from below the base of the mixed layer (discussed below). The S, A_T, and DIC mass balances are, respectively,

$$V_t\,\rho_t\,S_t = V_{sw}\,\rho_{sw}\,S_{sw} + V_{ice}\,\rho_{ice}\,S_{ice} \quad (2)$$

$$V_t\,\rho_t\,A_{Tt} = V_{sw}\,\rho_{sw}\,A_{Tsw} + V_{ice}\,\rho_{ice}\,A_{Tice} \quad (3)$$

$$V_t\,\rho_t\,DIC_t = V_{sw}\,\rho_{sw}\,DIC_{sw} + V_{ice}\,\rho_{ice}\,DIC_{ice} \quad (4)$$

where V is volume, ρ is density and the subscripts t, sw, and ice are the total, seawater, and ice values, respectively. The total values are the initial measured (S_t) or calculated (A_{Tt} and DIC_t) values at the 30-m sensor depth at the beginning of the time series. Ice density (ρ_{ice}) is assumed to be 900 kg/m^3 (Timco & Frederking, 1996) and seawater (ρ_{sw}) and total density (ρ_t) of the seawater and ice are assumed to equal 1,020 kg/m^3 (<0.7% error). These equations relate the total mass of S, A_T, and DIC to the mass of S, A_T, and DIC in each of the seawater and ice components. Volumes can be eliminated by substituting equation (2) into equations (3) and (4) and using conservation of mass $V_t\,\rho_t = V_{sw}\,\rho_{sw} + V_{ice}\,\rho_{ice}$, to yield

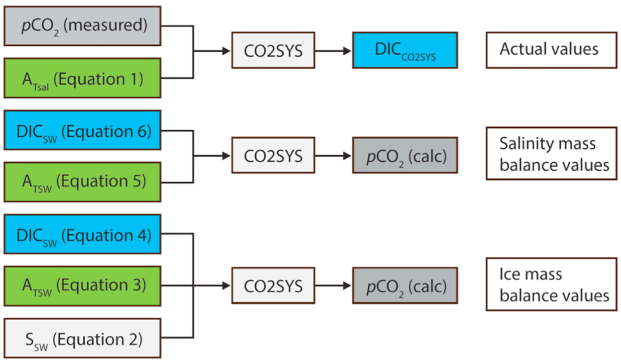

Figure 2. Flow chart of the CO2SYS and model calculations. The colors correspond to values that are compared in the model evaluation with "actual" (measured or directly calculated) values at top, salinity mass balance values in the middle, and ice mass balance values at bottom.

$$A_{Tsw} = A_{Tt} + \frac{S_{sw} - S_t}{S_t - S_{ice}}(A_{Tt} - A_{Tice}) \quad (5)$$

$$DIC_{sw} = DIC_t + \frac{S_{sw} - S_t}{S_t - S_{ice}}(DIC_t - DIC_{ice}) \quad (6)$$

In these equations, S_{sw}, the salinity time series, is used as a tracer for the A_T and DIC. One can see in equation (5) that if S_{ice} and A_{Tice} are zero, A_{Tt} changes proportionally to the change in salinity ($S_{sw} - S_t$) and equivalently for DIC (equation (6)), whereas during ice formation if some salt, A_T or DIC are retained in the ice, the changes in A_{Tsw} and DIC_{sw} are reduced. If ice retains the same concentrations as seawater, then there would be no change in A_T or DIC with ice formation. Note also that equation (5) will exactly predict A_{Tsalin} (equation (1)) for a specific A_{Tice} and S_{ice}, as discussed below.

In contrast, the ice mass balances use equations (3) and (4) directly with ice thickness determined by the ULS. Actual ice volume is not needed because volume ratios, that is, V_{ice}/V_{sw} and V_t/V_{sw}, are used which are equivalent to H_{ice}/H_{sw} and H_t/H_{sw}, the ratios of the thicknesses of the ice, seawater, and total (seawater + ice) layers where H_{sw} is mixed layer depth (MLD), above which all water properties are well mixed (constant). The MLD is defined here as the depth at which the density is 0.1 kg/m^3 or greater than the density at the surface.

For both the salinity and ice thickness based mass balances, we used S_{ice}, A_{Tice}, and DIC_{ice} values of 4.7, 415, and 330 μmol/kg, respectively, reported in Else et al. (2013) similar to the mean values found in first-year sea ice in Rysgaard et al. (2007). The sensitivity to these choices is evaluated below. We also assume that DIC is conserved between the ice and mixed layer and that no CO_2 is lost to the atmosphere. While some studies have shown significant efflux of CO_2 during ice formation based on eddy correlation (e.g., Miller et al., 2011), recently improved techniques have found no enhancement in air-ice fluxes during ice formation and fluxes decrease linearly with increasing ice coverage (Butterworth & Miller, 2016; Prytherch et al., 2017). The salinity and ice mass balance model results are evaluated by comparing the modeled A_{Tsw} and DIC_{sw} with the directly computed values (A_{Tsalin} and DIC_{CO2SYS}; Figure 2). In addition, the pCO_2 calculated from A_{Tsw} and DIC_{sw} for each model is compared to the measured pCO_2. The closeness of the predictions is examined by computing the slopes and correlation coefficients of the linear fit between DIC_{CO2SYS} and the modeled DIC through the period of ice formation (mid-April). The model results are focused on DIC rather than A_T because the results are very similar.

3. Results

3.1. Ship and Mooring Data

Ship CTD profiles obtained during mooring deployment and recovery are shown in Figure 3. The surface MLD was ~32 m at the beginning and 21 m at the end of the deployment. The temperature maximum at ~50- to 55-m depth is Pacific Summer Water (Aagaard et al., 1981; Toole et al., 2011). The shallower temperature peak evident during the mooring recovery is a characteristic of the near surface temperature maximum. It is observed in the summer and early fall and is due to the penetration of solar radiation (Jackson et al., 2011).

The mooring B time series data that are the focus of this study are shown in Figure 4. The pCO_2 sensor functioned successfully over the full mooring deployment making nearly 4,300 measurements. The pCO_2 was offset to match the initial pCO_2 measured by the ship's underway pCO_2 system during deployment. The pCO_2 measured on ITP 85, which drifted near the mooring in late December 2014, was 10 μatm lower than the mooring pCO_2. The pCO_2 calculated from A_T and DIC bottle samples upon recovery was 7 μatm lower than the mooring pCO_2. There was no indication of drift based on the instrument diagnostic data (Lai et al., 2018). Biofouling was also minimal.

The pressure recorded by the CTD sensor indicates that the mooring was periodically pushed down by eddies (Figure 4 depth record). We see mooring drawdown events in November, February and April that would

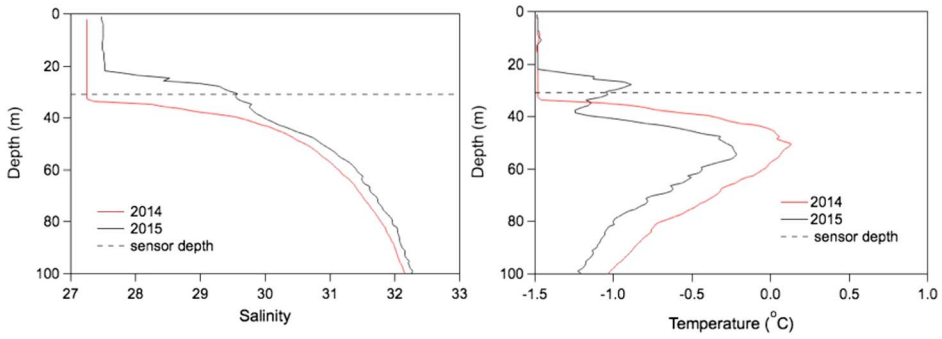

Figure 3. CTD salinity and temperature profiles obtained on deployment (9 October 2014; red) and recovery (29 September 2015; black) at the mooring B deployment location (Figure 1). The mean depth of the CTD, located just below the subsurface float, was 28.5 m, placing the pCO_2 sensor at ~30 m (horizontal dashed line). An increase in salinity and temperature were observed over the annual period (Figure 4).

appear to be associated with warm-core eddies consisting of water of Pacific origins via the Chukchi shelf where the pCO_2 is drawn down by biological production (Bates et al., 2014). The eddy event at the end of the record (late September) was more intense, pulling the sensors down hundreds of meters. In this case, the cooler, saltier, and higher pCO_2 water was likely a middepth eddy with its core at the base of the halocline formed at the front to the west of mooring B separating Eurasian and Canadian basin water types (Carpenter & Timmermans, 2012; Zhao & Timmermans, 2015). Notably, after the eddies departed, the time series resumed their pre-eddy trend.

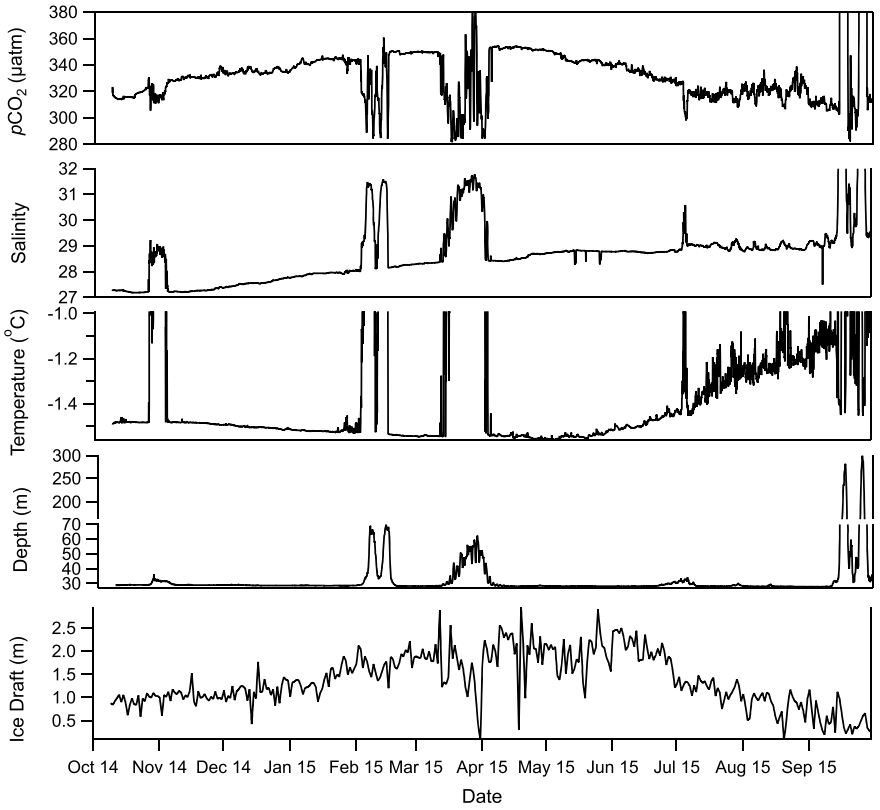

Figure 4. Mooring B time series collected from 9 October 2014 to 29 September 2015. The pCO_2 sensor was deployed at 30 m. Temperature and salinity were recorded by the CTD sensor at 28.5 m (see depth record in the fourth panel). Ice draft data are daily averages computed from the upward looking sonar located at 25 m. The sensor depth increased periodically due to strong eddy currents. Note that some of the sensor values are plotted off scale during these periods. The depth record has a split axis to better show the shallow depth excursions.

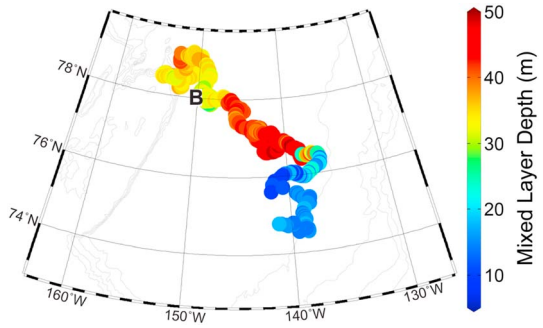

Figure 5. MLD (m) computed from CTD profiles from ITP 85 that drifted in the Canada Basin in a roughly northwest to southeast track. The ITP was deployed in the northwestern Canada Basin on 9 October 2014, to the northwest of Mooring B (location marked), and sampled until 1 September 2015; this is approximately the time window of the Mooring B time series (Figure 4). MLD was calculated based on the first value with depth in the CTD profile to exceed a density difference of 0.1 kg/m^3 from the top value. MLD ranged from around 30–40 m in the vicinity of Mooring B and to the northwest, increased to around 50 m when the ITP was in the central basin in winter (2014–15) then decreased to around 12–14 m in the southwestern-most part of the drift in summer 2015. Although there is some spatial variability, the general temporal trend is broadly consistent with past analyses of MLD in this region.

Ignoring these eddy periods, the pCO_2 steadily increased from ~315 to 350 μatm from the fall through winter, leveled off in late April and then returned close to its October 2014 value by late September. Salinity and ice draft show similar upward trends, slowly climbing then leveling off with maxima in late spring. Salinity and ice draft are correlated with pCO_2 through mid-April (r^2 = 0.77 and 0.62, respectively, not shown) omitting the eddy periods. Later in the period, however, pCO_2 and ice draft decreased, but salinity remained near its seasonal maximum until mooring recovery in September. This higher salinity water can also be seen in the CTD profile obtained during the mooring recovery (Figure 3). Temperature, omitting the eddy periods, tracked the freezing point dropping from −1.49 °C to −1.57 °C as the salinity increased until mid-June when solar warming began. Temperature increased by ~0.5 °C by the end of the deployment.

The ULS record represents the daily average distribution of ice draft as ice moves over the mooring location (Figure 4). Based on the ITP 85 positions, which drifted to within ±2° latitude and longitude of mooring B through early January (Figure 5), it was not uncommon for ice in this area to drift up to 30 cm/s, which is 26 km/day. The ULS record is highly variable because of nonuniform ice surfaces, that is, flat ice, ridges, and rafts, that passed over the mooring location. The 2014–2015 ULS record is typical of this location based on data analyzed from mooring B over a 9-year period (2003–2012; Krishfield et al., 2014). This study found mean maximum and minimum sea ice thickness of ~2.2 m in late spring and 0.5 m during summer, respectively. Sea ice typically increases slowly through the fall, winter and spring and then has a steep decline during summer.

3.2. Mixed Layer Depth

Knowledge of the MLD is important to determine the ratio of volumes used in equations (2)–(4) for the ice mass balance and to determine if the pCO_2 and CTD sensors were recording data in the mixed layer during the period of ice formation. Moreover, an increase in MLD could indicate entrainment at the base of the mixed layer, which would alter the salinity mass balance. As shown in Figure 3, the CTD and pCO_2 sensors were initially near the base of the mixed layer (32 m) and were within the pycnocline by the end of the deployment when the MLD was 20 m. ITP 85, which recorded T and S data up to ~9 m below the ice, indicates that the mixed layer ranged from ~30 to 34 m during the period when the ITP was near the mooring (through early January, Figure 5). Short-term variability of the pCO_2, T, and S records began to increase in mid-June, corresponding to the beginning of increasing temperature (Figure 4), suggesting that the sensors were in the pycnocline. Time series analysis of the pCO_2, T, and S records further supports increasing short-term variability in June. A 0.5-day period mooring motion shows up in the time-series as the sensors move up and down through the halocline (not shown). This 0.5-day period appears in the pCO_2 time series around 10 June 2015, supporting that the mixed layer had shoaled to less than 30 m. The mixed layer continued to shoal based on velocity sheer determined by the mooring ADCP (not shown). The mixed layer was deeper than the ADCP depth (~25 m) until approximately July 7 when it shoaled to ~10 m and then slowly increased to ~20 m by the end of the deployment. These observations are consistent with previous mixed layer depth records. In an analysis of 5,800 ITP profiles from 2003 to 2012 in the central Canada Basin, Toole et al. (2010) found that the mixed layer progressively deepened through early fall to reach its seasonal maximum of ~25 ± 10 m. The base of the mixed layer typically remained near this level through the winter but sometimes shoaled for brief periods due to processes such as water column heaving, lateral advection, and eddies. The mixed layer then more strongly shoaled in early summer commonly to less than 10 m between June and July. These combined observations support that the pCO_2 and CTD sensors were in the mixed layer through the ice formation period, judged to be through approximately mid-April based on the ice draft record. For the mass balance, we used the mean MLD recorded by ITP 85 through early January (34 ± 3 m). The sensitivity to this value is discussed below.

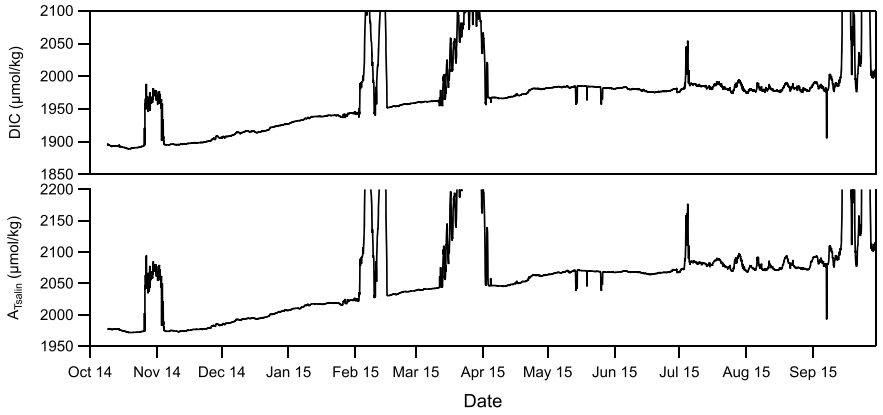

Figure 6. Time series of calculated A_{Tsalin} and DIC_{CO2SYS}. A_{Tsalin} was calculated using the salinity alkalinity relationship in equation (1). DIC_{CO2SYS} was calculated from A_{Tsalin} and the measured pCO_2 using the in situ temperature and salinity (Figure 2 flowchart; Figure 4 data). Values are plotted off-scale during some periods when the mooring was drawn deeper by passing eddies (see text).

3.3. Directly Calculated and Modeled Parameters

As stated in section 2, A_{Tsalin} was calculated with the relationship in equation (1). DIC was then calculated in CO2SYS using A_{Tsalin}, the measured pCO_2, temperature, and salinity (DIC_{CO2SYS}, Figure 2). The resulting A_{Tsalin} and DIC_{CO2SYS} time series are shown in Figure 6. The initial A_{Tsalin} and DIC_{CO2SYS} values were within 10 µmol/kg of the 22-m bottle samples taken during the deployment. Upon mooring recovery, bottle samples were collected at 22- and 43-m depth that bracketed the sensor depth (which was below the mixed layer depth at this time as shown in Figure 3 and discussed above). The A_{Tsalin} and DIC_{CO2SYS} fell between these values, that is for A_T, the 22 m, 30-m mooring, and 43-m values are 1,987, 2,110, 2,143 µmol/kg, respectively, and for DIC are 1,905, 2,005, and 2,036 µmol/kg, respectively. Thus, A_{Tsalin} and DIC_{CO2SYS} are consistent with directly measured values.

In Figure 6, it is seen that A_{Tsalin} increased from 1,976 to 2,115 µmol/kg and DIC_{CO2SYS} from 1,893 to 2,010 µmol/kg between deployment and recovery. The DIC did not decrease in late spring like the pCO_2 (Figure 4) because most of the DIC increase came from the increase in A_{Tsalin}. The drop in DIC due to pCO_2 alone was 17 µmol/kg based on comparing the DIC computed with a constant pCO_2 with DIC_{CO2SYS}.

The correlations between pCO_2, S, and ice draft suggest that ice formation could be driving the increase in pCO_2. This process was investigated using the mass balance methodology described above. The parameters used in the models and resulting statistics are shown in Table 1. The salinity mass balance, using the values from Else et al. (2013), initially closely follows the trend of rising DIC but overpredicts the DIC over the course of the ice formation period (Figure 7, Case 1 in Table 1). No retention of S, A_T, or DIC in ice, that is, setting all ice values to 0, does not significantly change the mass balance from Case 1 (Case 2, Table 1).

Table 1
Parameters Used in the Mass Balances

Parameter	Case 1	Case 2	Case 3	Case 4	Case 5	Case 6	Case 7	Case 8	Case 9
MLD (m)	>30	>30	>30	>30	34	34	30	40	34
S_{ice}	4.7	0	4.7	4.7	4.7	0	4.7	4.7	4.7
A_{Tice} (µmol/kg)	415	0	640	415	415	0	415	415	640
DIC_{ice} (µmol/kg)	330	0	580	300	330	0	330	330	580
A_{Tice}:DIC_{ice}	1.25	NA	1.1	1.38	1.25	NA	1.38	1.38	1.1
slope, r^2 for DIC	1.17, 0.96	1.17, 0.96	0.98, 0.96	1.19, 0.96	0.70, 0.78	0.83, 0.78	0.80, 0.78	0.60, 0.78	0.69, 0.78
slope, r^2 for pCO_2	0.89, 0.77	0.58, 0.77	0.68, 0.77	1.05, 0.77	0.73, 0.71	0.49, 0.74	0.79, 0.71	0.66, 0.72	0.52, 0.74

Note. The shaded headers are the salinity-based mass balances (equations (5) and (6)). The clear headers are the ice-based mass balances (equations (2)–(4)) using the upward looking sonar data. Correlations are for the ice formation period (October to mid-April). See section 2 for a detailed description. Results are plotted for some cases in Figure 7. NA = not applicable.

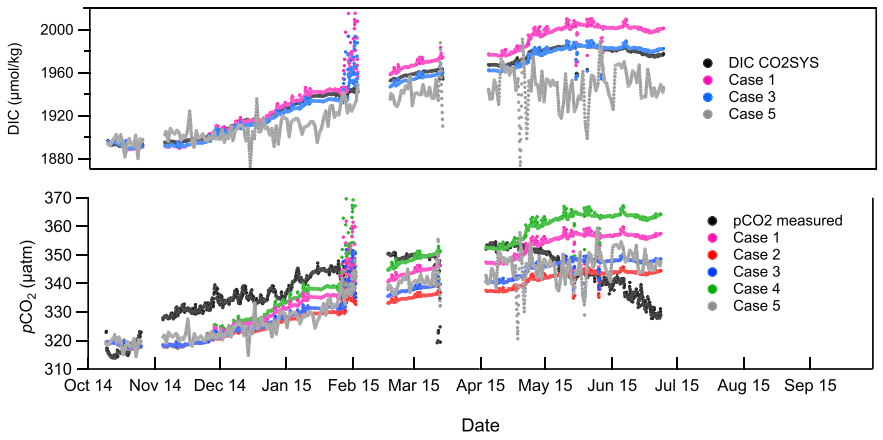

Figure 7. Mass balance model results for DIC (top) and pCO_2 (bottom) for different parameter settings (Case 1–9, Table 1). The pCO_2 was calculated from the DIC and A_T mass balances. Some cases are omitted because they closely overlay other cases. Data are cutoff after the mixed layer shoaled in early July during ice melt. Model-data comparisons (bottom of Table 1) only include data between October 2014 and mid-April 2015. Periods when the mooring was drawn down by eddies are also excluded.

We also optimized the least squares fit by varying A_{Tice} assuming a ratio of A_{Tice}:DIC_{ice} of 1.1 (Rysgaard et al., 2007) and keeping $S_{ice} = 4.7$ (Case 3). This fit estimates A_{Tice} and DIC_{ice} to be 640 and 580 μmol/kg, respectively and closely follows DIC_{CO2SYS} (Figure 7 and Table 1) and A_{Tsalin} (not shown). In this case, the fit converges on an A_{Tice} value close to the endmember value that would be predicted from Equation (1) (617 μmol/kg for $S = 4.7$). It is not exactly equal to the Equation (1) value because of the A_{Tice}:DIC_{ice} constraint. Cases 2 and 4 (discussed below) essentially overlap Case 1 and are therefore not shown in Figure 7.

The ice draft mass balance using the Else et al. (2013) parameters also follows the general upward trend of DIC during the ice formation period (Case 5, Figure 7, and Table 1). The variability is much larger than the salinity mass balance because of the large short-term changes recorded by the ULS. Unlike the salinity mass balance, the ice mass balance underpredicts the rise in DIC comparing Case 1 and Case 5 that have the same ice values (Table 1). Assuming ice values are 0 (100% excluded, Case 6) brings the prediction closer (slope = 0.83, Table 1, not shown in Figure 7 for clarity). The least squares fit of A_{Tice}, as done for Case 3 in the salinity mass balance, converges on $A_{Tice} = DIC_{ice} = 0$ because these values give the highest predicted value of DIC and A_T (Case 6). Decreasing the mean MLD increases the predicted DIC because it concentrates the excluded solutes in a smaller volume—with a MLD of 30 m the slope = 0.80 (Case 7). Conversely, the values further underpredict DIC if a 40-m MLD is used (Case 8). Using the least squares fit values from the salinity mass balance (Case 3), further underpredicts the ice mass balance because more DIC is retained in the ice (Case 9).

The salinity and ice mass balances both follow the observed trend of rising inorganic carbon through the ice formation period. The results are sensitive to the amount of inorganic carbon that is retained in the ice, comparing Case 1 and Case 3 salinity mass balances (Figure 7 and Table 1 slope and r^2 for DIC) or Case 5 and Case 9 ice mass balances (Table 1), but the reasonably good DIC predictions for the two independent mass balance approaches support that ice exclusion significantly increased DIC (and A_T, not shown) concentrations in the sea surface. It is also important to determine if the mass balance modeled A_T and DIC can predict the observed fall to winter increase in pCO_2 (Figure 4), as evaluated in the following paragraph.

The mass balance-modeled DIC and A_T and measured T and S were used to compute the pCO_2 for all of the cases shown in Table 1. All of the modeled DIC and A_T combinations predict an increase in pCO_2 through the ice formation period, a few examples of which are shown in Figure 7. There is an early November step change in the measured pCO_2 that is not predicted by the mass balances, but the different models all indicate a rise in pCO_2 through the winter and spring. The pCO_2 prediction is, however, sensitive to the A_{Tice}:DIC_{ice} ratio. Case 1, with an A_{Tice}:DIC_{ice} ratio of 1.25, predicts a pCO_2 that increases at a similar rate to that

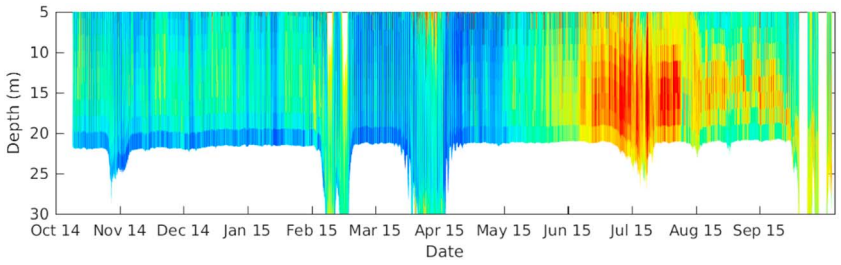

Figure 8. Acoustic Doppler current profiler (ADCP) backscatter record (relative scale with blue being the lowest and red being the highest relative intensity) from Mooring B during the 2014–2015 deployment. ADCP echo intensity was corrected for sound absorption and beam attenuation to generate relative backscatter as described in Klevjer et al. (2012). The ADCP depth was ~25 m.

observed (Figure 7). Although Case 3 with higher A_{Tice} and DIC_{ice} gave an excellent prediction of DIC, the pCO_2 computed from this pair significantly underestimates the pCO_2 likely because of its low A_{Tice}:DIC_{ice} ratio (1.1). A higher A_{Tice}:DIC_{ice} ratio (Case 4, 1.38) compared to Case 1 and Case 3 gave a more rapid increase in pCO_2 than that observed. The A_T:DIC ratio of 1.8 reported in Rysgaard et al. (2009) would further over predict the pCO_2 and therefore does not appear representative of the ice conditions in this study. No increase in pCO_2 occurs if A_{Tice}:DIC_{ice} ratio is 0.8, although ratios less than 1 are rarely observed (Rysgaard et al., 2007). It is evident that the observed increase in pCO_2 can result from ice exclusion and that the magnitude is primarily dependent upon the ratio of A_T and DIC retained in the ice rather than the amount of DIC in the ice. If less DIC is retained in the ice relative to A_T, a larger increase in pCO_2 is predicted because the DIC will increase more in the mixed layer relative to A_T. Importantly, however, the increase in pCO_2 still occurs if 100% of the A_T and DIC are excluded (Case 2), essentially equivalent to the process of evaporation in open water environments.

3.4. Post Ice Formation Period

The pCO_2 began to decline in late April (Figure 4). The beginning of this decrease is coincident with a leveling off of salinity and ice draft. In mid-May, the ADCP record shows that particle backscatter began to increase (transition of relative backscatter from blue to light green), presumably due to zooplankton responding to a phytoplankton bloom (Figure 8; Flagg & Smith, 1989). The pCO_2 continued to decrease until mid-July after the zooplankton signal had been at a high level for a couple of weeks and remained high through mid-August. While ikaite particles from melting ice might be large enough (Rysgaard et al., 2013) to also have a backscatter signal, the pCO_2 began to decrease well before significant ice melt occurred where ikaite could dissolve and reduce the pCO_2. Warming of the surface ocean also began in early summer with an increase of ~0.5 °C by the end of the deployment. This warming would increase the pCO_2 by ~7 μatm. Based on inorganic carbon calculations, the calculated pCO_2 drawdown (~40 μatm including correction for warming) corresponds to a DIC loss of ~17 μmol/kg, as noted previously. These observations suggest that the drawdown in pCO_2 was regulated by biological production and grazing prior to and during the ice melt period. The loss of DIC corresponds to a net community production (NCP) of 7 ± 3 mmol m^{-2} day^{-1} assuming a mean MLD of 25 m and a 60-day drawdown period from mid-May to mid-July where the uncertainty (± 3 mmol $\bullet m^{-2} \bullet$ day^{-1}) is based on the range of MLD from 20 to 30 m and drawdown from 60 to 90 days. There are almost no reports of NCP that overlap this region during winter and spring. NCP was 2–4 mmol$\bullet$ $m^{-2}\bullet$ day^{-1} in late summer 2015 when the mooring was recovered (Ji et al., 2019). The low salinity surface waters in the Canada Basin are generally without measurable nitrate during the summer (Brown et al., 2015). There was no nitrate above 40 m based on bottle samples collected during the deployment and recovery. The observed spring and summer new production might be sustained by reduced forms of nitrogen (Varela et al., 2013).

4. Discussion and Conclusions

During the ice formation period, A_T and DIC increased by 75 and 74 μmol/kg, respectively, the pCO_2 increased by ~35 μatm (Figures 4 and 6) and salinity increased from 27.2 to 28.5. The mass balance

models support that these increases can be primarily attributed to exclusion from growth of ~1.0–1.5 m of ice (Figure 4) during the fall to winter of 2014–2015. Using different parameters in the mass balances shows that the increase in mixed layer DIC is somewhat sensitive to the amount of DIC retained in the ice and is sensitive to the mixed layer depth. The pCO_2 that results depends strongly on the ratio of A_T and DIC in the ice. Similar monotonic increases in salinity have been attributed to sea ice formation (Shcherbina et al., 2003). Other ITP and mooring data that we have collected often show increases in pCO_2 and S during the ice formation period (e.g., pCO_2 and S measured by ITP 85 increased by 30 μatm and 0.2, respectively, from late October to late December 2014). The observation of ice exclusion is often obscured when the sensors are deployed deeper than the mixed layer, as has been the case for most of our Canada Basin deployments since 2014.

Other mechanisms that could increase DIC include net respiration, entrainment of high DIC and A_T water from the base of the mixed layer and lateral advection of higher DIC water. Respiration could play a small role in modifying the observed change in DIC, but this cannot explain the increase in salinity and the proportional increase in A_T that comes with it. A_T cannot be altered significantly by respiration because the release of CO_2 adds neither an acid nor a base. Entrainment alone could not increase salinity nor inorganic carbon as much as observed. A mixed layer deepening from 30 to 40 m would result in a 0.3 unit salinity change, using the profile data from the deployment (Figure 3), corresponding to about 23% of the observed salinity increase and, therefore, only a 23% increase in A_T would be possible. Entrainment might, however, explain why the ULS data (e.g., using Case 5) underestimate the A_T and DIC increase. It will be insightful to account for entrainment in future studies where direct mixed layer observations are available. Lateral advection was also not accounted for here. Although the estimated 1-D balances would seem to suggest that the influences of lateral advection are secondary, there remains the possibility that surface Ekman processes (see Proshutinsky et al., 2009) transport anomalous A_T and DIC into the region. Efforts to quantify this would also be useful extensions of the 1-D study presented here.

The ultimate fate of the A_T and DIC is not clear. The small portion of DIC (~15%) taken up by biological production might find its way to deeper waters through sinking particles and zooplankton migration. During the fall, the mixed layer should deepen and mix the low-density ice melt water with this higher-density, high DIC water, further lowering the pCO_2 (Rysgaard et al., 2007) and increasing air-sea uptake of CO_2. Unfortunately, we did not deploy a CO_2 sensor on Mooring B in 2015 to observe this transition. The Canada Basin is not like the Atlantic sector of the AO where brine and inorganic carbon can sink deep into the water column because strong stratification is not present (Maksym, 2019; Rysgaard et al., 2007, 2011, 2009). Lateral export of the surface water, for example, through Fram Strait, could lead to conditions where deep water formation and inorganic carbon export are possible. Right now, it appears that in the perennially ice-covered central AO the DIC and A_T is seasonally trapped above the pycnocline. However, export of inorganic carbon deeper into the water column is likely to increase with the loss of perennial ice cover in the AO. Expanding regions of open water in summer (Barnhart et al., 2016) due to melting and increased ice export (Maksym, 2019) will lead to more seasonal ice production (Shcherbina et al., 2003) and wind energy input into the upper ocean, which can increase pycnocline mixing and export of CO_2 to deeper waters. Thus, like most other physical and biogeochemical processes in the AO, the inorganic carbon cycle will be changing, posing major challenges for characterizing and understanding these processes in the years ahead.

Acknowledgments
Research Associate Cory Beatty (University of Montana) prepared the CO_2 instruments and helped with the mooring deployments and data processing. Pierce Fix (undergraduate intern, University of Montana) helped with the mass balance modeling. The moorings were designed and deployed by personnel at Woods Hole Oceanographic Institution. Michiyo Yamamoto-Kawai (University of Tokyo) and Marty Davelaar (Institute of Ocean Sciences; IOS) provided the alkalinity and dissolved inorganic carbon data. We thank the captain, officers, crew, and chief scientists (Bill Williams and Sarah Zimmerman, IOS) of the CCGS Louis S. St. Laurent. The data used in this study are available through the U.S. National Science Foundation (NSF) Arctic Data Center (https://arcticdata.io). This research was made possible by grants from the NSF Arctic Observing Network program (ARC-1107346, PLR-1302884, PLR-1504410, and PLR-1723308).

References

Aagaard, K., Coachman, L., & Carmack, E. (1981). On the halocline of the Arctic Ocean. *Deep Sea Research*, *28*(6), 529–545. https://doi.org/10.1016/0198-0149(81)90115-1

Anderson, L. G., & Macdonald, R. W. (2015). Observing the Arctic Ocean carbon cycle in a changing environment. *Polar Research*, *34*(1). https://doi.org/10.3402/polar.v34.26891

Arrigo, K. R., & van Dijken, G. L. (2015). Continued increases in Arctic Ocean primary production. *Progress in Oceanography*, *136*, 60–70. https://doi.org/10.1016/j.pocean.2015.05.002

Barnhart, K. R., Miller, C. R., Overeem, I., & Kay, J. E. (2016). Mapping the future expansion of Arctic open water. *Nature Climate Change*, *6*(3), 280–285. https://doi.org/10.1038/nclimate2848

Bates, N. R., Garley, R., Frey, K., Shake, K., & Mathis, J. T. (2014). Sea-ice melt CO_2-carbonate chemistry in the western Arctic: Meltwater contributions to air-sea CO_2 gas exchange, mixed layer properties and rates of net community production. *Biogeosciences*, *11*(23), 6769–6789. https://doi.org/10.5194/bg-11-6769-2014

Bates, N. R., Moran, S. B., Hansell, D. A., & Mathis, J. T. (2006). An increasing CO_2 sink in the Arctic Ocean due to sea-ice loss. *Geophysical Research Letters*, *33*, L23609. https://doi.org/10.1029/2006GL027028

Bergeron, M., & Tremblay, J.-É. (2014). Shifts in biological productivity inferred from nutrient drawdown in the southern Beaufort Sea (2003–2011) and northern Baffin Bay (1997–2011), Canadian Arctic. *Geophysical Research Letters*, *41*, 3979–3987. https://doi.org/10.1002/2014GL059649

Bouttes, N., Paillard, D., & Roche, D. M. (2010). Impact of brine-induced stratification on the glacial carbon cycle. *Climate of the Past*, *6*(5), 575–589. https://doi.org/10.5194/cp-6-575-2010

Brown, Z. W., Casciotti, K. L., Pickart, R. S., Swift, J. H., & Arrigo, K. R. (2015). Aspects of the marine nitrogen cycle of the Chukchi Sea shelf and Canada Basin. *Deep-Sea Research Part II: Topical Studies in Oceanography*, *118*, 73–87. https://doi.org/10.1016/j.dsr2.2015.02.009

Butterworth, B. J., & Miller, S. D. (2016). Air-sea exchange of carbon dioxide in the Southern Ocean and Antarctic marginal ice zone. *Geophysical Research Letters*, *43*, 7223–7230. https://doi.org/10.1002/2016GL069581

Cai, W., Chen, L., Chen, B., Gao, Z., Lee, S. H., Chen, J., et al. (2010). Decrease in the CO_2 uptake capacity in an ice-free Arctic Ocean basin. *Science*, *329*(5991), 556–559. https://doi.org/10.1126/science.1189338

Carpenter, J. R., & Timmermans, M.-L. (2012). Deep mesoscale eddies in the Canada Basin, Arctic Ocean. *Geophysical Research Letters*, *39*, L20602. https://doi.org/10.1029/2012GL053025

DeGrandpre, M., Evans, W., Timmermans, M.-L., Krishfield, R., Proshutinsky, A., Steele, M., & Williams, W. (2019). Changes in the Arctic Ocean carbon cycle with diminishing ice cover, in revision.

DeGrandpre, M. D., Hammar, T. R., Smith, S. P., & Sayles, F. L. (1995). In situ measurements of seawater pCO_2. *Limnology and Oceanography*, *40*(5), 969–975. https://doi.org/10.4319/lo.1995.40.5.0969

Dickson, A. G., & Millero, F. J. (1987). A comparison of the equilibrium constants for the dissociation of carbonic acid in seawater media. *Deep Sea Research Part A. Oceanographic Research Papers*, *34*(10), 1733–1743. https://doi.org/10.1016/0198-0149(87)90021-5

Dieckmann, G. S., Nehrke, G., Papadimitriou, S., Göttlicher, J., Steininger, R., Kennedy, H., et al. (2008). Calcium carbonate as ikaite crystals in Antarctic sea ice. *Geophysical Research Letters*, *35*, L08501. https://doi.org/10.1029/2008GL033540

Else, B. G. T., Papakyriakou, T. N., Galley, R. J., Mucci, A., Gosselin, M., Miller, L. A., et al. (2012). Annual cycles of pCO_{2sw} in the southeastern Beaufort Sea: New understandings of air-sea CO_2 exchange in arctic polynya regions. *Journal of Geophysical Research*, *117*, C00G13. https://doi.org/10.1029/2011JC007346

Else, G. T., Galley, R. J., Lansard, B., Barber, D. G., Brown, K., Miller, L. A., et al. (2013). Further observations of a decreasing atmospheric CO_2 uptake capacity in the Canada Basin (Arctic Ocean) due to sea ice loss. *Geophysical Research Letters*, *40*, 1132–1137. https://doi.org/10.1002/grl.50268

Evans, W., Mathis, J. T., Cross, J. N., Bates, N. R., Frey, K. E., Else, B. G. T., et al. (2015). Sea-air CO_2 exchange in the western Arctic coastal ocean. *Global Biogeochem. Cycles*, *29*, 1190–1209. https://doi.org/10.1002/2015GB005153

Flagg, C. N., & Smith, S. L. (1989). On the use of the acoustic Doppler current profiler to measure zooplankton abundance. *Deep Sea Research*, *36*(3), 455–474. https://doi.org/10.1016/0198-0149(89)90047-2

Fransson, A., Chierici, M., Miller, L. A., Carnat, G., Shadwick, E., Thomas, H., et al. (2013). Impact of sea-ice processes on the carbonate system and ocean acidification at the ice-water interface of the Amundsen Gulf, Arctic Ocean. *Journal of Geophysical Research: Oceans and Atmospheres*, *118*, 7001–7023. https://doi.org/10.1002/2013JC009164

Geilfus, N.-X., Galley, R. J., Else, B. G. T., Campbell, K., Papakyriakou, T., Crabeck, O., et al. (2016). Estimates of ikaite export from sea ice to the underlying seawater in a sea ice–seawater mesocosm. *The Cryosphere*, *10*, 2173–2189.

Islam, F., DeGrandpre, M., Beatty, C., Krishfield, R., & Toole, J. (2016). Gas exchange of CO_2 and O_2 in partially ice-covered regions of the Arctic Ocean investigated using in situ sensors. *IOP Conference Series: Earth and Environmental Science*, *35*. https://doi.org/10.1088/1755-1315/35/1/012018 012018

Islam, F., DeGrandpre, M., Beatty, C., Timmermans, M.-L., Krishfield, R., Toole, J., & Laney, S. (2017). Sea surface pCO_2 and O_2 dynamics in the partially ice-covered Arctic Ocean. *Journal of Geophysical Research: Oceans*, *122*, 1425–1438. https://doi.org/10.1002/2016JC012162

Jackson, J. M., Allen, S. E., McLaughlin, F. A., Woodgate, R. A., & Carmack, E. C. (2011). Changes to the near-surface waters in the Canada Basin, Arctic Ocean from 1993–2009: A basin in transition. *Journal of Geophysical Research*, *116*, C10008. https://doi.org/10.1029/2011JC007069

Ji, B. Y., Sandwith, Z. O., Williams, W. J., Diaconescu, O., Ji, R., Li, Y., et al. (2019). Variations in Rates of Biological Production in the Beaufort Gyre as the Arctic Changes: Rates from 2011 to 2016. *Journal of Geophysical Research: Oceans*, *124*. https://doi.org/10.1029/2018JC014805

Jutterström, S., & Anderson, L. G. (2010). Uptake of CO_2 by the Arctic Ocean in a changing climate. *Marine Chemistry*, *122*(1-4), 96–104. https://doi.org/10.1016/j.marchem.2010.07.002

Klevjer, T. A., Torres, D. J., & Kaartvedt, S. (2012). Distribution and diel vertical movements of mesopelagic scattering layers in the Red Sea. *Marine Biology*, *159*(8), 1833–1841. https://doi.org/10.1007/s00227-012-1973-y

Krishfield, R., Toole, J., Proshutinsky, A., & Timmermans, M.-L. (2008). Automated ice-tethered profilers for seawater observations under pack ice in all seasons. *Journal of Atmospheric and Oceanic Technology*, *25*(11), 2091–2105. https://doi.org/10.1175/2008JTECHO587.1

Krishfield, R. A., Proshutinsky, A., Tateyama, K., Williams, W. J., Carmack, E. C., McLaughlin, F. A., & Timmermans, M.-L. (2014). Deterioration of perennial sea ice in the Beaufort Gyre from 2003 to 2012 and its impact on the oceanic freshwater cycle. *Journal of Geophysical Research: Oceans*, *119*, 1271–1305. https://doi.org/10.1002/2013JC008999

Lai, C.-Z., DeGrandpre, M., & Darlington, R. (2018). Autonomous optofluidic chemical analyzers for marine applications: Insights from the Submersible Autonomous Moored Instruments (SAMI) for pH and pCO_2. *Frontiers in Marine Science*, *4*. https://doi.org/10.3389/fmars.2017.00438

Maksym, T. (2019). Arctic and Antarctic sea ice change: Contrasts, commonalities, and causes. *Annual Review of Marine Science*, *11*(1), 187–213. https://doi.org/10.1146/annurev-marine-010816-060610

Mehrbach, C., Culberson, C. H., Hawley, J. E., & Pytkowicz, R. M. (1973). Measurement of the apparent dissociation constants of carbonic acid in seawater at atmospheric pressure. *Limnology and Oceanography*, *18*(6), 897–907. https://doi.org/10.4319/lo.1973.18.6.0897

Miller, L. A., Papakyriakou, T. N., Collins, R. E., Deming, J. W., Ehn, J. K., Macdonald, R. W., et al. (2011). Carbon dynamics in sea ice: A winter flux time series. *Journal of Geophysical Research*, *116*, C02028. https://doi.org/10.1029/2009JC006058

Moreau, S., Vancoppenolle, M., Bopp, L., Aumont, O., Madec, G., Delille, B., et al. (2016). Assessment of the sea-ice carbon pump: Insights from a three-dimensional ocean-sea-ice biogeochemical model (NEMO-LIM-PISCES). *Elementa: Science of the Anthropocene*, *4*. 000122

Petrich, C., & Eicken, H. (2010). Growth, structure and properties of sea ice. In D. N. Thomas & G. S. Dieckmann (Eds.), *Sea ice*, (second ed. pp. 23–78). Oxford, UK: Wiley-Blackwell.

Pierrot, D., Lewis, E., & Wallace, D. W. R. (2006). MS Excel program developed for CO_2 system calculations. In *ORLN/CDIAC-105, Carbon Dioxide Information Analysis Center, Oak Ridge National Laboratory, US*. Oak Ridge, Tennessee: Department of Energy. https://doi.org.10.3334/CDIAC/otg.CO2SYSXLSCDIAC105a

Proshutinsky, A., Krishfield, R., & Barber, D. (2009). Preface to special section on Beaufort Gyre Climate System Exploration Studies: Documenting key parameters to understand environmental variability. *Journal of Geophysical Research*, *114*, C00A08. https://doi.org/10.1029/2008JC005162

Prytherch, J., Brooks, I. M., Crill, P. M., Thornton, B. F., Salisbury, D. J., Tjernström, M., et al. (2017). Direct determination of the air-sea CO_2 gas transfer velocity in Arctic sea ice regions. *Geophysical Research Letters*, *44*, 3770–3778. https://doi.org/10.1002/2017GL073593

Robbins, L. L., Wynn, J. G., Lisle, J. T., Yates, K. K., Knorr, P. O., Byrne, R. H., et al. (2013). Baseline monitoring of the western Arctic Ocean estimates 20% of Canadian Basin surface waters are undersaturated with respect to aragonite. *PLoS ONE*, *8*, e73796. https://doi.org/10.1371/journal.pone.0073796

Rysgaard, S., Bendtsen, J., Delille, B., Dieckmann, G. S., Glud, R. N., Kennedy, H., et al. (2011). Sea ice contribution to the air-sea CO_2 exchange in the Arctic and Southern Oceans. *Tellus*, *63B*, 823–830.

Rysgaard, S., Bendtsen, J., Pedersen, L. T., Ramløv, H., & Glud, R. N. (2009). Increased CO_2 uptake due to sea ice growth and decay in the Nordic Seas. *Journal of Geophysical Research*, *114*, C09011. https://doi.org/10.1029/2008JC005088

Rysgaard, S., Glud, R. N., Lennert, K., Cooper, M., Halden, N., Leakey, R. J. G., et al. (2012). Ikaite crystals in melting sea ice—Implications for pCO_2 and pH levels in Arctic surface waters. *The Cryosphere*, *6*, 901–908. https://doi.org/10.5194/tc-6-901-2012

Rysgaard, S., Glud, R. N., Sejr, M. K., Bendtsen, J., & Christensen, P. B. (2007). Inorganic carbon transport during sea ice growth and decay: A carbon pump in polar seas. *Journal of Geophysical Research*, *112*, C03016. https://doi.org/10.1029/2006JC003572

Rysgaard, S., Søgaard, D. H., Cooper, M., Pućko, M., Lennert, K., Papakyriakou, T. N., et al. (2013). Ikaite crystal distribution in winter sea ice and implications for CO_2 system dynamics. *The Cryosphere*, *7*(2), 707–718. https://doi.org/10.5194/tc-7-707-2013

Shcherbina, A. Y., Talley, L. D., & Rudnick, D. L. (2003). Direct observations of North Pacific ventilation: Brine rejection in the Okhotsk Sea. *Science*, *302*(5652), 1952–1955. https://doi.org/10.1126/science.1088692

Timco, G. W., & Frederking, R. M. W. (1996). A review of sea ice density. *Cold Regions Science and Technology*, *24*(1), 1–6. https://doi.org/10.1016/0165-232X(95)00007-X

Timmermans, M.-L., Krishfield, R., Laney, S., & Toole, J. (2010). Ice-tethered profiler measurements of dissolved oxygen under permanent ice cover in the Arctic Ocean. *Journal of Atmospheric and Oceanic Technology*, *27*, 1936–1949. https://doi.org/10.1175/2010JTECHO772.1

Toole, J. M., Krishfield, R. A., Timmermans, M.-L., & Proshutinsky, A. (2011). The ice-tethered profiler: Argo of the Arctic. *Oceanography*, *24*, 126–135. https://doi.org/10.5670/oceanog.2011.64

Toole, J. M., Timmermans, M.-L., Perovich, D. K., Krishfield, R. A., Proshutinsky, A., & Richter-Menge, J. A. (2010). Influences of the ocean surface mixed layer and thermohaline stratification on Arctic Sea ice in the central Canada Basin. *Journal of Geophysical Research*, *115*, C10018. https://doi.org/10.1029/2009JC005660

Varela, D. E., Crawford, D. W., Wrohan, I. A., Wyatt, S. N., & Carmack, E. C. (2013). Pelagic primary productivity and upper ocean nutrient dynamics across Subarctic and Arctic Seas. *Journal of Geophysical Research: Oceans*, *118*, 7132–7152. https://doi.org/10.1002/2013JC009211

Yamamoto-Kawai, M., McLaughlin, F. A., & Carmack, E. C. (2011). Effects of ocean acidfication, warming and melting of sea ice on aragonite saturation of the Canada Basin surface water. *Geophysical Research Letters*, *38*, L03601. https://doi.org/10.1029/2010GL045501

Yamamoto-Kawai, M., Tanaka, N., & Pivovarov, S. (2005). Freshwater and brine behaviors in the Arctic Ocean deduced from historical data of $\delta^{18}O$ and alkalinity (1929-2002 A.D.). *Journal of Geophysical Research*, *110*, C10003. https://doi.org/10.1029/2004JC002793

Yasunaka, S., Murata, A., Watanabe, E., Chierici, M., Fransson, A., van Heuven, S., et al. (2016). Mapping of the air–sea CO_2 flux in the Arctic Ocean and its adjacent seas: Basin-wide distribution and seasonal to interannual variability. *Polar Science*, *10*, 323–334. https://doi.org/10.1016/j.polar.2016.03.006

Zhao, M., & Timmermans, M.-L. (2015). Vertical scales and dynamics of eddies in the Arctic Ocean's Canada Basin. *Journal of Geophysical Research: Oceans*, *120*, 8195–8209. https://doi.org/10.1002/2015JC011251